Non-parabolicity and band gap re-normalisation in Si doped ZnO

R. E. Treharne, L. J. Phillips, K. Durose, A. Weerakkody, I. Z. Mitrovic, and S. Hall
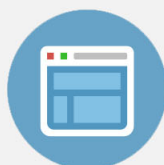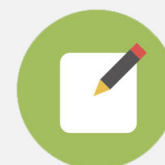
Non-parabolicity and band gap re-normalisation in Si doped ZnO

R. E. Treharne,[1,a] L. J. Phillips,[1] K. Durose,[1] A. Weerakkody,[2] I. Z. Mitrovic,[2] and S. Hall[2]

[1]*Stephenson Institute for Renewable Energy, University of Liverpool, Liverpool, United Kingdom*
[2]*Department of Electrical Engineering and Electronics, University of Liverpool, Liverpool, United Kingdom*

A combinatorial methodology, developed for the rapid optimisation of sputtered transparent conducting oxides, was applied to Si doped ZnO. A wide range of compositions have been explored over a single sample to determine an optimum composition, with respect to the minimisation of resistivity, of $x = 0.65\%$ wt. SiO_2. A fundamental investigation of the conduction band non-parabolicity yields values of $m_{e0} = 0.35m_0$ and $C = 0.3\,eV^{-1}$ for the conduction band minimum effective mass and the non-parabolicity factor, respectively. The variation of extracted band gap values with respect to dopant concentration provided an estimate of the magnitude of re-normalization effects. A model is proposed to describe the carrier transport behaviour for a degenerate polycrystalline semiconductor by accounting for the tunnelling of carriers through grain boundaries. © *2014 AIP Publishing LLC*. [http://dx.doi.org/10.1063/1.4863875]

I. INTRODUCTION

Polycrystalline ZnO films have received significant attention in recent years. They can be degenerately doped, typically by incorporating group III (e.g., Al, Ga, or In (Ref. 1)) or group VII (e.g., F (Refs. 2 and 3) and Cl (Ref. 4)) elements to achieve resistivities of the order of $10^{-4}\,\Omega\,cm$, while maintaining high optical transparency (>80%). Such ZnO based transparent conducting oxide (TCO) films, most notably Al doped ZnO (AZO), are now used extensively within thin-film photovoltaic technologies, particularly CIGS, CZTS, and CdTe, and have widely replaced the use of indium based TCOs. A wide range of deposition techniques have been demonstrated for ZnO films including atomic layer deposition (ALD),[5] metal-organic chemical vapour deposition (MOCVD),[6] pulsed laser deposition (PLD),[7] and magnetron sputtering.[1,8,9]

The key property of a TCO is its resistivity, which in the context of thin-film photovoltaics (PV), should be as low as possible. Optical transmittance will generally remain high over the visible wavelength range for a wide range of resistivities, except in the case of exceptionally high free carrier concentrations (i.e., $>10^{21}\,cm^2$), and so is of secondary concern experimentally. The most common approach to the experimental minimisation of TCO resistivity is to generate large sample sets over which a single experimental parameter (e.g., pressure, temperature, doping density) is varied incrementally. Such investigations are time consuming and the experimental consistency from sample to sample can be poor due to uncontrolled drifts in other associated deposition parameters. Furthermore, in cases where the resistivity is highly sensitive, it may vary over several orders of magnitude for a narrow composition range and it is possible to miss the resistivity minimum when using the conventional approach.

An alternative approach is the combinatorial methodology in which single large sample plates are grown for which there is a spatial variation in either the major element composition or the doping density. Knowledge of the spatial composition variation may then be combined with the results of spatially resolved electrical conductivity measurements (from probes or optical methods) to yield the complete compositional dependence of the electrical properties of the material system for a given set of deposition conditions. This has been demonstrated for the case of ZnO:Al (Ref. 10) for which $100 \times 100\,mm^2$ plates were coated by co-sputtering.

In this work, the usefulness of the combinatorial method for TCOs is extended by using it to explore and exploit knowledge of the functional dependence of band structure and electron transport properties on carrier concentration. The method is shown to give information on conduction band non-parabolicity and band gap re-normalisation. The metal-oxide system chosen for application of the combinatorial methodology was silicon doped zinc oxide (SZO). SZO remains a relatively under-studied transparent conductor, although it has recently received specific attention from Rougier *et al.*,[11–13] who has demonstrated the potential for fine tuning of the doping concentration by co-sputtering from separate ZnO and SiO_2 targets. A key objective of this work was to determine, with high accuracy, the relationship between the dopant concentration and the opto-electronic characteristics of the material. Theoretically, Si should act as a tetravalent dopant in ZnO and contribute two electrons to the conduction band for each incorporated Si atom. This is verified experimentally for the first time in this work. Also, the investigation of the relationship between mobility and carrier concentration demonstrates that the carrier transport mechanisms within the material are dominated by grain boundary scattering: this suggests ways of generating high mobility TCOs.

II. EXPERIMENTAL METHODS

Films were deposited by RF magnetron sputtering using an AJA Phase II-J Orion system. The system was configured

a)Author to whom correspondence should be addressed. Electronic mail: R.Treharne@liverpool.ac.uk

in a "sputter-up" geometry with the substrate being suspended above two separate ceramic targets of ZnO and SiO$_2$ arranged off-centre and tilted at 5° towards the centre of the substrate. Soda-lime glass substrates (OptiWhite$^{\text{TM}}$, NSG Pilkington) of size $100 \times 100 \times 4$ mm^3 were cleaned by scrubbing with a nylon brush and a series of de-ionized water and isopropanol alcohol rinses followed by blow drying with a nitrogen gas jet. During deposition, the ZnO and SiO$_2$ targets were sputtered simultaneously using powers of 150 W and 50 W, respectively. A growth pressure of 2.7×10^{-3} mbar Ar was used during deposition. The substrate temperature was maintained at 350 ± 5 °C during growth and the substrate was not rotated. Note that the chosen substrate temperature was determined, through preliminary investigations, to be optimum for minimising resistivity in SZO films. Deliberate gradients of both thickness and composition were, therefore, incorporated across the resultant film to generate a "combinatorial" sample. A second film of pure SiO$_2$ was deposited under identical conditions (but without ZnO) to generate a reference film for estimating the % wt. profile of SiO$_2$ in the co-sputtered combinatorial sample.

A Shimadzu UV-Vis-IR 3700 spectrophotometer with mapping capability was used to measure the transmittance of the co-sputtered film over the range of 250–2500 nm. A total of 289 spectra were taken in total at 5 mm increments over the full sample surface. At each of these 289 points, the sheet resistance was also measured using a CMT-SR2000 4-point probe mapping system. Following transmittance and sheet resistance measurements, the sample was cut into one hundred 10×10 mm^2 pieces. A selection of these pieces, 10 in total, were further scribed into four 5×5 mm^2 sections and Hall measurement was performed on each of them. Hall measurements were performed with custom built equipment (Semimetrics Ltd), using a field strength of 0.8 T. Ellipsometry was performed on the same sections using a Woollam M2000-UI system. Ellipsometry was also used to map the thickness profile of the pure SiO$_2$ reference film.

III. RESULTS

A. Fitting of optical spectra

Figure 1 shows a typical transmittance spectrum taken from a single point on the combinatorial ZnO:Si sample and the corresponding fit achieved using a theoretical model[10] of the dielectric permittivity $\varepsilon(\omega)$. The key components of the model include: a Lorentzian oscillator to account for the behaviour of the system's bound electrons and to provide a smoothly varying dielectric background over the range of interest (250–2500 nm), an extended Drude model,[14] to characterise the system's free electron response, and an inter-band transition model to account for the steep increase in the absorption coefficient in the vicinity of the direct band gap (3.3–3.4 eV). The two key parameters extractable from the dielectric model are the film's thickness, d, and the plasma frequency, ω_p, which is related directly to the carrier concentration according to

$$\omega_p = \sqrt{\frac{n_e e^2}{m_e \varepsilon_\infty \varepsilon_0}}, \qquad (1)$$
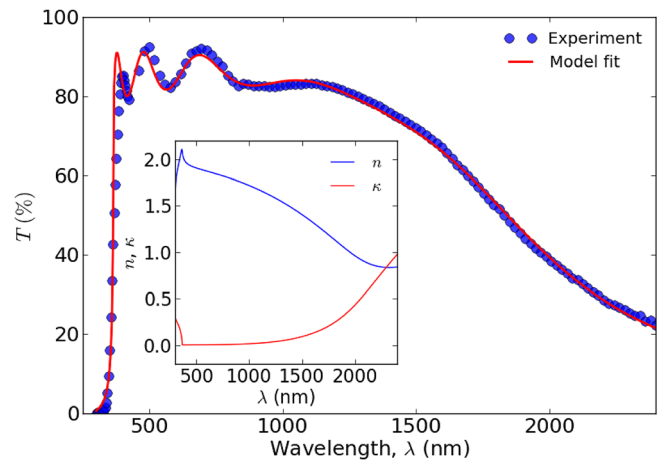

FIG. 1. Example of a typical transmittance curve taken from a single point on the combinatorial ZnO:Si sample. The line shows the fit generated from the dielectric model.[10] An excellent fit is achieved at wavelengths in the vicinity of plasma edge, i.e., >1000 nm but the band to band transition component of the model is insufficient to accurately describe the behaviour in the vicinity of the direct band gap. In this instance, values of $d = 518 \pm 10$ nm, $\varepsilon_\infty^{1/2}\omega_p = 0.97 \pm 0.02$ eV, and $E_G = 3.38 \pm 0.04$ eV were extracted from the fitting procedure. The inset also shows the dispersion relationships for n and κ extracted using the model.

where m_e is the effective mass of the electrons (expressed in units of the free electron mass, m_0), ε_∞ is the high frequency relativity permittivity ($\sim$8.3 for single crystal ZnO (Ref. 15)), and ε_0 is the permittivity of free space. Note that as ε_∞ is not known for the specific sample, the combined product $\varepsilon_\infty^{1/2}\omega_p$ was extracted as a single parameter from the model and here-in the term "plasma frequency" refers to this product. The optical dispersion for the material, i.e., refractive index n and extinction coefficient κ, was also extracted from the fitting procedure and the spectra are shown in the inset of Figure 1.

Fitting was achieved by using a Nelder-Mead downhill simplex algorithm,[16] implemented via python script, to minimize the quantity

$$\chi^2 = \sum_i^N \sqrt{\frac{y_i - O_i}{N^2}}, \qquad (2)$$

where N is the total number of data points in the spectra, O_i the observed transmittance at each wavelength over the range of interest, and y_i the theoretical transmittance calculated using the transfer matrix method[17] for a single thin-film on a finite, transparent substrate. The fitting algorithm was iterated until the relative fractional change in consecutive χ^2 values was less than 1×10^{-6}. The fitting of all 289 transmittance spectra taken over the combinatorial sample was fully automated; the only user input required being an initial estimate of film thickness at the point of the first spectrum. This automation ensured that the fitting of consecutive spectra was highly consistent. For all spectra, χ^2 values of <2 were achieved indicating that all fits were as successful as that shown in Figure 1.

It was not possible to extract values for the true optical band gap E_G from the inter-band transition component of the model which relied on a simple $\alpha \propto (E - E_G)^{1/2}$ dependence to

describe the behaviour in the vicinity of the band edge. All values of E_G were typically $\sim 0.2 - 0.4\,\text{eV}$ lower than expected, even when non-parabolicity and re-normalisation effects had been accounted for (see Secs. III B and III C). This could be explained by the presence of a population of impurity states located in energy just below the bottom of the conduction band. The presence of these states generates a broadening, commonly referred to as an "Urbach tail,"[18] in the onset of the absorption coefficient. It is very difficult to determine the extent of this broadening by fitting the dielectric model to a single transmittance spectrum. The use of variable angle ellipsometry permitted a more reliable extraction of the band gap values due to the requirement that the fitting procedure satisfied multiple spectra simultaneously.

For each point over the combinatorial sample, ellipsometric spectra were taken at angles of 65 and 70° with respect to a plane normal to the sample surface. The spectra were fitted using a parameterized semiconductor (PSEMI-M0) model[19] over the range of 350–1000 nm. Figure 2(a) shows a typical fit achieved by the model to ellipsometric data and Figure 2(b) shows the difference in the α^2 versus E behaviour extracted from transmittance and ellipsometry data, respectively. This disparity between band gaps extracted from the two techniques is in good agreement with that reported by Srikant[20] for ZnO.

B. Conduction band non-parabolicity

For highly doped metal-oxides, it has been shown that the conduction band, E_c, is non-parabolic and that this may be attributed to a carrier dependent effective mass, $m_e(n_e)$. The functional form of this dependence, first suggested by Pisarkiewicz *et al.*,[21] is given by
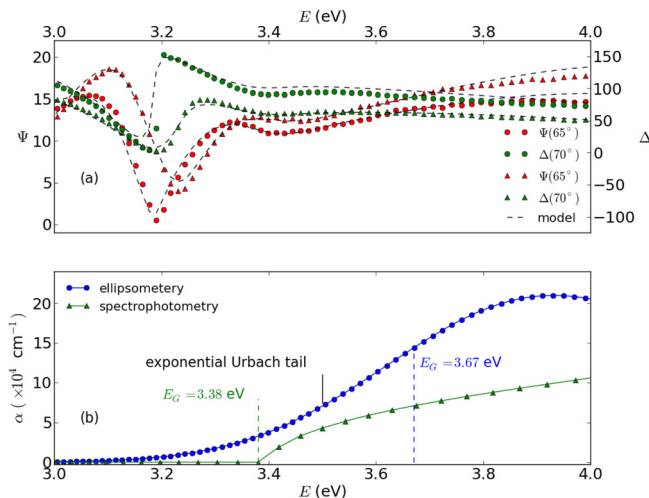
$$m_e(n_e) = m_{e0}\sqrt{1 + \frac{2C\hbar^2 k}{m_{e0}}}, \qquad (3)$$

where m_{e0} is the value of the effective mass at the conduction band minimum and C is the non-parabolicity factor, expressed in eV^{-1}. The carrier wave-number can be expressed in terms of the carrier concentration according to $k = (3\pi^2 n_e)^{1/3}$. By re-examining Eq. (1), it is clear that the relationship between ω_p^2 and n_e becomes non-linear if the effective mass is not a constant. Figure 3 shows a plot of ω_p, extracted from the spectrophotometry measurements, versus the carrier concentration, n_e^H, determined from Hall measurements, for the sample subset cut from the original combinatorial sample. A similar χ^2 minimization procedure to that described in Sec. III A, in which the fitting parameters were m_{e0} and C, was applied to the data set using

$$\chi^2 = \sum_{i=1}^{N} \frac{(n_{e_i}^S - n_{e_i}^H)^2}{N^2}, \qquad (4)$$

where the superscript S corresponds to carrier concentrations calculated using a carrier dependent effective mass $m_e(n_e)$ obtained from the spectroscopically determined plasma frequencies (Eqs. (1) and (3)). The superscript H denotes values of n_e determined directly from Hall measurements. To determine the uncertainty associated with the fitted m_{e0} and C values, Monte-Carlo style error treatment[22] was implemented within which the χ^2 minimization procedure was performed 1000 times. The inset plot in Figure 3 shows the mean $m_e(n_e)$ relationship (solid line) and the corresponding spread (shaded line). The average extracted value of $m_{e0} = 0.35 \pm 0.04\,m_0$ is
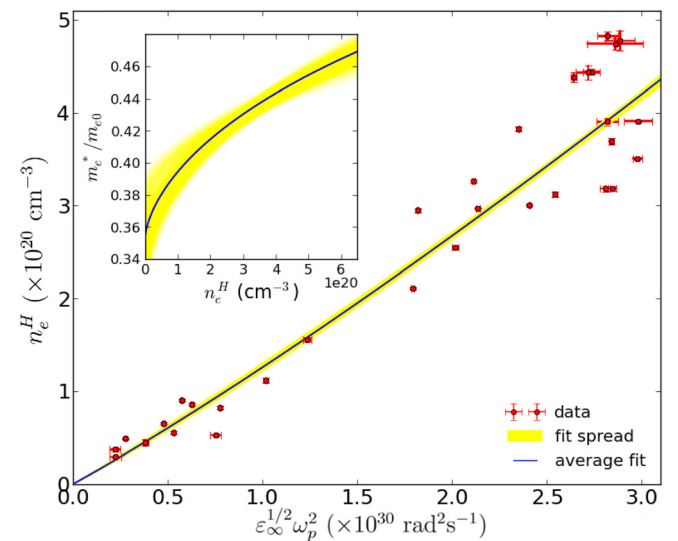

FIG. 2. (a) Ellipsometric spectra (Ψ and Δ), measured at separate angles of 65° and 70°, were fitted over the range 3 eV (413 nm) to 4 eV (309 nm) using a single PSEMI-M0 oscillator.[19,36] (b) The corresponding absorption coefficient extracted from the ellipsometric data compared with that extracted from the spectrophotometric data (1). A difference in the direct band gap of ~ 0.3 eV is determined between the two optical extraction methods. The ellipsometric model is deemed to be more reliable due to its ability to account for the Urbach tail that arises from a distribution of impurity states located just below the bottom of the conduction band.

FIG. 3. Carrier concentration, n_e^H, determined from Hall effect measurements versus values of $\varepsilon_\infty \omega_p^2$ extracted from the dielectric modeling of transmittance data. A Monte-Carlo fitting procedure[22,37] indicates that the relationship between the axes is non-linear, as expected for a material with a non-parabolic conduction band. The spread in uncertainty associated with the fitting procedure is shown by the shaded line. The corresponding relationship between the carrier effective mass, m_e and the carrier concentration is shown in the inset. Values of $m_{e0} = 0.35 \pm 0.04\,m_0$ and $C = 0.30 \pm 0.03\,\text{eV}^{-1}$ were extracted from the analysis.

higher than previous published values of $0.24 - 0.28m_0$ for the effective mass in undoped ZnO. An average extracted value of $C = 0.30 \pm 0.03\,\text{eV}^{-1}$ agrees very well with previously reported values of $\sim 0.29\,\text{eV}^{-1}$ for Al doped ZnO films.[9,23]

C. Band gap re-normalization

The optical band gap of a degenerately doped metal-oxide system increases as a function of carrier concentration (Burstein-Moss shift)[24,25] according to

$$E_G = E_{G0} + \frac{\hbar^2 (3\pi^2 n_e)^{2/3}}{2m_{JDOS}}, \tag{5}$$

where E_{G0} is the band gap at the conduction band minimum and the joint density of states effective mass, m_{JDOS} is given as

$$\frac{1}{m_{JDOS}} = \frac{1}{m_h} + \frac{1}{m_e(n_e)}. \tag{6}$$

A constant hole effective mass value of $m_h = 0.7m_0$ (Refs. 26 and 27) is assumed throughout this work. Note that the non-parabolicity of the conduction band is accounted for when estimating the band gap by the use of the carrier dependent effective mass $m_e(n_e)$ determined in Sec. III B. The data points in Figure 4 show the band gap values, determined from ellipsometry, plotted against the Hall carrier concentrations. The points lie some distance from the relationship predicted by Eq. (5). The apparent reduction in the real band gap values is due the re-normalization effects of many body electron-electron, electron-ion, and electron-hole interactions. Lu *et al.*[28] have shown that the total energy shift due to re-normalization can be estimated by parameterising the detailed model described by Jain *et al.*[29,30] according to

$$E_R = An_e^{1/3} + Bn_e^{1/4} + Cn_e^{1/2}, \tag{7}$$

where E_R is negative with respect to E_G. The $n_e^{1/3}$, $n_e^{1/4}$, and $n_e^{1/2}$ dependencies correspond to the exchange energy of free electrons, their correlation energy, and the electron-ion interaction energy, respectively. The coefficients A, B, and C quantify the strength of each of these three dependencies. The coefficient values and a value for E_{G0} were extracted using the established minimisation procedure. Table I shows the extracted values and comparative values for n-type ZnO thin-films. The strength of the $n_e^{1/3}$ dependence is roughly three times that reported for Al doped ZnO but values for the other two coefficients are consistent.[28]

IV. MAPPING OF COMPOSITIONAL DEPENDENCIES

Film thickness profiles were determined for the combinatorial ZnO:Si and SiO$_2$ samples. The % wt. SiO$_2$ content at each point over the combinatorial sample was estimated according to

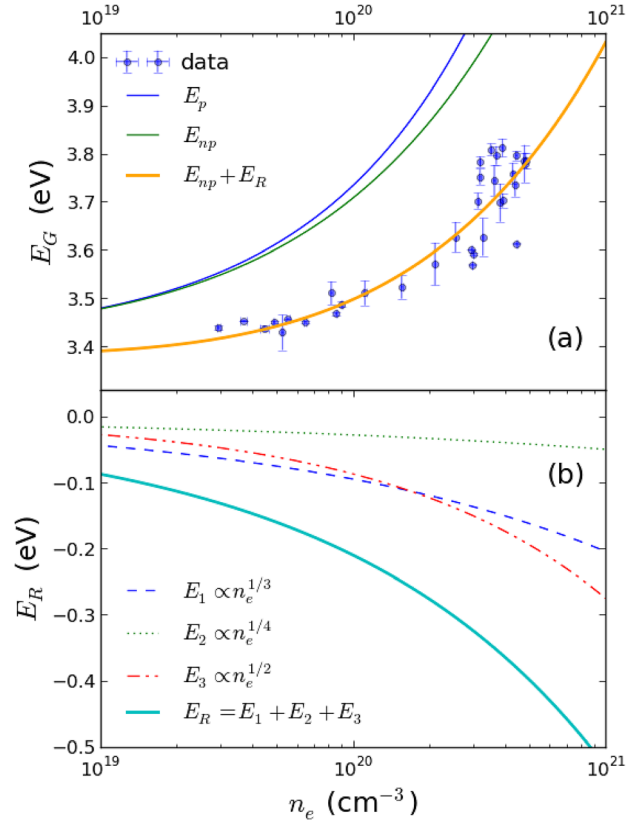$$x = \frac{\Gamma_B d_B}{\Gamma_A d_A + \Gamma_B d_B} \times 100\%, \tag{8}$$

FIG. 4. (a) Band gap (from ellipsometry) values, E_G, plotted with respect to the carrier concentration determined by Hall measurements. The Burstein-Moss relation (E_p), even when non-parabolicity is accounted for (E_{np}), is insufficient to predict the observed relationship, the band gap values being significantly lower than expected. The incorporation of re-normalization effects permits the data to be fitted. (b) The total re-normalization energy and each of its sub-components are shown. The amplitude of these components is calculated empirically via a Monte-Carlo fitting procedure using the model proposed by Jain.[29]

where Γ_A and Γ_B are the bulk densities of ZnO and SiO$_2$, respectively, and d_A and d_B are the corresponding thicknesses, d, of the ZnO and SiO$_2$ films. The carrier concentration profile for the combinatorial sample was calculated from extracted $\varepsilon_\infty^{1/2}\omega_p$ values according to Eq. (1) and using the non-parabolic effective mass relationship, $m_e(n_e)$, determined in Sec. III B. The corresponding mobility profile was calculated using

$$\mu_e = \frac{1}{n_e^S R_S de}, \tag{9}$$

TABLE I. Parameter values extracted from the downhill-simplex fit of Eq. (7) to the experimental data shown in Figure 4. E_G values were extracted from fits to ellipsometry spectra taken in the vicinity of the band gap and n_e values were determined by Hall measurements. The coefficients A, B, and C correspond to the amplitudes of the separate $n_e^{1/3}$, $n_e^{1/4}$, $n_e^{1/2}$ dependencies, respectively, of the renormalisation effects.

Parameter 1	Extracted value	Comparison[28]
A ($\times 10^{-8}$ eV cm)	2.1 ± 0.8	0.69
B ($\times 10^{-7}$ eV cm$^{3/2}$)	3.0 ± 2.6	1.6
C ($\times 10^{-7}$ eV cm$^{3/4}$)	8.7 ± 1.5	7.76
E_{G0} (eV)	3.41 ± 0.01	...

where R_S is the sheet resistance obtained directly from four point probe measurements. Figure 5 shows the three dimensional contour profiles of n_e and μ_e across the surface of the combinatorial sample. In both cases, a maximal ridge, corresponding to $n_e \sim 4.5 \times 10^{20}$ cm^{-3} an $\mu_e \sim 16$ cm^2 V^{-1} s^{-1}, runs diagonally across the sample. By superimposing the contour distribution of x (dotted black contour lines), a very strong correlation between carrier concentration and composition becomes apparent, the maximum n_e and μ_e values corresponding to a value of $x = 0.65\%$ and a minimum resistivity of 8.6×10^{-4} Ω.cm. These values are comparable to those obtained by Rougier *et al.*[13] for SZO. Compared to AZO films, the resistivity of SZO reported here is typically twice as high. However, with further optimisation of deposition conditions, most notably substrate temperature and sputter pressure, it is very likely that similar electrical performances can be achieved in SZO films.

By plotting the distributions of n_e and μ_e with respect to x, the compositional dependencies can be observed directly as shown in Figure 6. Here, the strength of the combinatorial analysis is fully appreciated by its ability to generate continuous, non-ambiguous distributions of the electrical behaviour and shows that it is highly sensitive to composition—the

resistivity spanning over three orders of magnitude within the compositional range $x = 0\% - 0.65\%$. Furthermore, the uncertainty in the optimum value of x, that minimises the resistivity, is significantly reduced when compared to the multi-sample analyses that are commonly reported.

The solid straight line in the n_e vs x plot indicates the relationship predicted for a 100% doping efficiency, i.e., where every Si atom incorporated into film substitutionally replaces a Zn atom and contributes two free electrons to the system. For low values of x, i.e., in the range $x = 0\% - 0.5\%$, this relationship is adhered to. However, as x increases further the doping efficiency decreases rapidly and the carrier concentration is limited to $3 - 4 \times 10^{20}$ cm^{-3} for compositions up to 10% wt. SiO$_2$. After the optimum value of x is reached, the mobility drops off, steeply at first, and reaching a level of ~ 2 cm^2 V^{-1} s^{-1} for $x > 6\%$. This suggests that as x is increased beyond the optimum composition Si does not incorporate substitutionally but rather at a site or phase where it contributes to impurity scattering but not the carrier concentration.
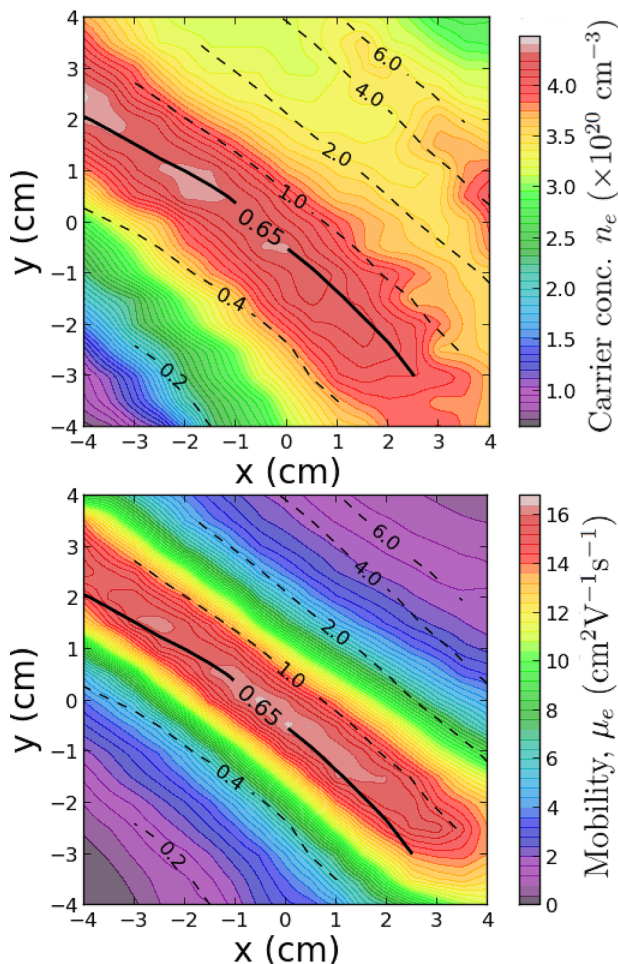

FIG. 5. Contour plots of the carrier concentration and mobility over the combinatorial sample. All values were extracted using the automated spectrophotometric mapping procedure. The (- - -) contour lines show an overlay of the % wt. SiO$_2$ composition profile.
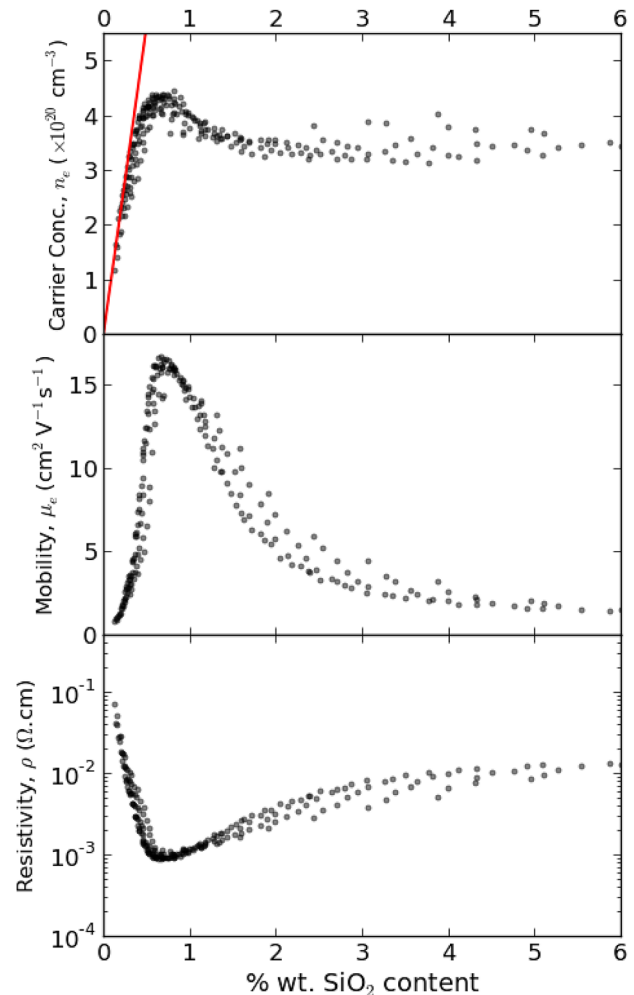

FIG. 6. Dependencies of carrier concentration, mobility, and resistivity with respect to % wt. SiO$_2$ content. The maximum values for n_e (4.4×10^{20} cm^{-3}) and μ_e (16.5 cm^2 V^{-1} s^{-1}) coincide with a composition of 0.65% wt. SiO$_2$ and correspond to a minimum resistivity of 8.6×10^{-4} Ω.cm. The solid straight line in the top plot shows the carrier concentration expected if every Si atom incorporated onto a zinc site contributes exactly two free electrons to the system.

V. SCATTERING

The behaviour of carrier mobility can be described further by considering its direct relationship with the carrier concentration. Figure 7 shows that by plotting μ_e versus n_e for all data points in the range $0\% < x < 0.65\%$ a well defined, unambiguous relationship is determined. The data points correspond to compositions $x < 0.65\%$. Within this distribution, and for carrier concentrations below 3×10^{20} cm^{-3}, the mobility of the free carriers can be described in terms of the grain barrier limited transport model proposed by Seto *et al.*[31] The model assumes that at the grain boundaries a population of filled and charged trap states exists within the band gap. This causes the conduction band to bend upwards at each grain boundary forming a barrier to charge transport. The inter-grain mobility, μ_{ig}, of free carriers is therefore limited by thermal processes according to

$$\mu_{ig} = \mu_0 \exp\left(-\frac{\Phi_B}{k_B T}\right), \quad (10)$$

where Φ_B is the barrier height at the grain boundary and is related directly to the carrier concentration according to

$$\Phi_B = \frac{e^2 n_t}{8\varepsilon_\infty \varepsilon_0 n_e}, \quad (11)$$

where n_t is the trap density. The pre-factor μ_0 is the internal mobility of the grain, expressed as

$$\mu_0 = \frac{eL}{\sqrt{2\pi m_e k_B T}}, \quad (12)$$

where L is the grain size. It is necessary to extend the Seto model in the case of degenerately doped ZnO to account for the tunnelling of carriers through the barrier Φ_B. As the carrier concentration increases, the Fermi level rises towards the top of the barrier, while the barrier height decreases in proportion to $1/n_e$. Following the onset of tunnelling, the effective carrier mobility increases exponentially with respect to carrier concentration. The increase in mobility is eventually limited by the next most dominant scattering process, i.e., ionized impurity scattering. A semi-empirical relationship for the mobility, that incorporates the effects due to the tunnelling of free carriers, is proposed as

$$\mu_{ig} = \mu_0 \left[\exp\left(\frac{-\Phi_B}{k_B T}\right) + \exp\left(\frac{\Delta_{BM} + E_R - 2\Phi_B}{k_B T}\right)\right], \quad (13)$$

where Δ_{BM} is the Burstein-Moss shift, as given by the second term in Eq. (5), and E_R is the total re-normalization energy as calculated in Sec. III C. The second exponential term in the expression, which describes the tunnelling behaviour of the free carriers, is consistent with the model proposed by Bruneaux *et al.*,[32] following the application of Fermi-Dirac statistics to a degenerately doped, polycrystalline system. The overall effective mobility, μ_{eff}, may be calculated by combining μ_{ig} with the mobility due to scattering from ionized impurities, μ_{ii}, according to Mattheisen's rule, as the two mechanisms are uncorrelated,

$$\frac{1}{\mu_{eff}} = \frac{1}{\mu_{ig}} + \frac{1}{\mu_{ii}}. \quad (14)$$

Figure 7 shows the corresponding fit of Eqs. (10)–(14) to the data. A constant value of μ_{ii} was used during the fitting procedure. This is an adequate approximation as μ_{ii} will only show a significant contribution to μ_{eff} in the range $n_e < 3 \times 10^{20}$ cm^{-3} and is likely to vary slowly with respect to the tunnelling term of Eq. (13) for concentrations $>3 \times 10^{20}$ cm^{-3}.

The fitting extracts a parameter value for the grain boundary trap density of $n_t = 3.1 \times 10^{14}$ cm^{-3}. This value is more than two orders of magnitude higher than reported for reactively sputtered, undoped ZnO films[33] and an order of magnitude greater than that for Al doped ZnO films.[34] This is reflected in the relatively low mobility values in the range $n_e < 3 \times 10^{20}$ cm^{-3} compared with Al doped ZnO thin films. For $n_e > 3 \times 10^{20}$ cm^{-3}, carrier tunnelling through grain boundaries leads to an exponential increase in μ_{eff}. The continued increase in μ_{eff} with respect to n_e is limited by ionized impurity scattering, which caps the mobility at ~ 19 cm^{2}V^{-1}s^{-1}. A key route to attaining higher effective mobilities in TCOs is by increasing μ_{ii}. Work by Gessert *et al.*[35] suggests that by incorporating group V transition elements, such as V and Nb, into the metal-oxide matrix the level of ionized impurities can be controlled. Pursuing further investigations that involve the incorporation of other transition metal dopants is a promising line of inquiry for the development of high-mobility TCOs.
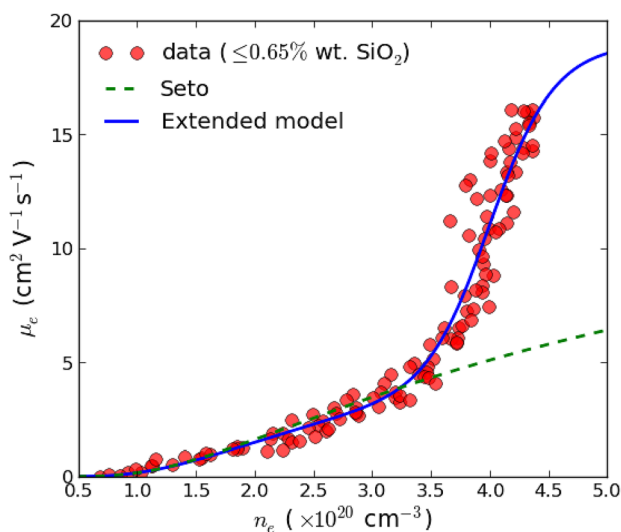
FIG. 7. Relationship between n_e and μ_e values extracted from the automated spectrophotometric mapping procedure. All data points have compositions below and up to the optimum value of 0.65% wt. SiO$_2$. The line (—) shows the fit achieved to the data using Eqs. (10)–(14). The parameter values $n_t = 2.1 \times 10^{14}$ cm^2, $L = 98$ nm, and $\mu_{ii} = 19$ cm^{2}V^{-1}s^{-1} were extracted from the fitting procedure.

VI. CONCLUSIONS

A consideration of the non-parabolicity of the conduction band for Si doped ZnO has yielded estimates for the

values of the band minimum effective mass, $m_{e0} = 0.35m_0$, and the non-parabolicity factor, $C = 0.3\,\text{eV}^{-1}$. The non-parabolicity contributes to a reduction in the expected Burstein-Moss shift of the optical band gap at carrier concentrations beyond $10^{20}\,\text{cm}^{-3}$. Further reductions in the band gap arise from the re-normalization effects, which are dominated by electron-electron and electron-ion interactions. For Si doped films, the magnitude of these effects is significantly greater than that reported for sputtered Al doped ZnO films.

The combinatorial methodology employed within this work allowed the relationship between composition and the electrical behaviour to be determined accurately, yielding continuous distributions between n_e, μ_e, ρ, and % wt. SiO_2. Furthermore, the extraction of all data from a single sample ensured that a high level of consistency between each data point was achieved compared to that possible for measurements taken over a series of separately deposited samples. Maximum values of $4.5 \times 10^{20}\,\text{cm}^{-3}$ and $16\,\text{cm}^2\,\text{V}^{-1}\,\text{s}^{-1}$ were achieved for the carrier concentration and mobility, respectively, at an optimal composition of $x = 0.65\%$ wt. SiO_2, corresponding to a minimum resistivity of $8.7 \times 10^{-4}\,\Omega\,\text{cm}$.

The model of grain boundary scattering proposed by Seto[31] has been extended to include the effects of tunnelling through grain boundaries. The model generates a good agreement for the observed μ_e versus n_e behaviour at compositions up to the optimum value of x. The model highlights a potential route to improving carrier mobility, i.e., by controlling the density of ionized impurities.

ACKNOWLEDGMENTS

[1]T. Minami, Semicond. Sci. Technol. **20**, S35 (2005).
[2]J. Hu and R. Gordon, Sol. Cells **30**, 437 (1991).
[3]R. E. Treharne and K. Durose, Thin Solid Films **519**, 7579 (2011).
[4]J. Rousset, E. Saucedo, and D. Lincot, Chem. Mater. **21**, 534 (2009).
[5]P. R. Chalker, P. A. Marshall, S. Romani, J. W. Roberts, S. J. C. Irvine, D. A. Lamb, A. J. Clayton, and P. A. Williams, J. Vac. Sci. Technol. A **31**, 01A120 (2013).
[6]S. Y. Myong, S. J. Baik, C. H. Lee, W. Y. Cho, and K. S. Lim, Jpn. J. Appl. Phys., Part 2 **36**, L1078 (1997).
[7]S.-M. Park, T. Ikegami, K. Ebihara, P.-K. Shin, T. Park, T. Ikegami, K. Ebihara, and P.-K. Shin, Appl. Surf. Sci. **253**, 1522 (2006).
[8]T. Minami, T. Miyata, Y. Ohtani, and Y. Mochizuki, Jpn. J. Appl. Phys., Part 2 **45**, L409 (2006).
[9]K. Ellmer, J. Phys. D: Appl. Phys. **34**, 3097 (2001).
[10]R. E. Treharne, K. Hutchings, D. A. Lamb, S. J. C. Irvine, D. Lane, and K. Durose, J. Phys. D: Appl. Phys. **45**, 335102 (2012).
[11]J. Clato, G. Campet, A. Zeiner, C. Labrugère, M. Nister, and A. Rougier, Sol. Energy Mater. Sol. Cells **95**, 2357 (2011).
[12]C. Faure, J. Clatot, L. Teulé-Gay, G. Campet, C. Labrugère, M. Nistor, and A. Rougier, Thin Solid Films **524**, 151 (2012).
[13]J. Clatot, M. Nistor, and A. Rougier, Thin Solid Films **531**, 197 (2013).
[14]D. Mergel and Z. Qiao, J. Phys. D: Appl. Phys. **35**, 794 (2002).
[15]N. Ashkenov, B. N. Mbenkum, C. Bundesmann, V. Riede, M. Lorenz, D. Spemann, E. M. Kaidashev, A. Kasic, M. Schubert, and M. Grundmann, J. Appl. Phys. **93**, 126 (2003).
[16]J. A. Nelder and R. Mead, Comput. J. **7**, 308 (1965).
[17]H. A. Macleod, *Thin-Film Optical Filters* (Adam Hilger Ltd, 1986).
[18]F. Urbach, Phys. Rev. **92**, 1324 (1953).
[19]C. Herzinger, B. Johs, W. McGahan, J. Woollam, and W. Paulson, J. Appl. Phys. **83**, 3323 (1998).
[20]V. Srikant and D. R. Clarke, J. Appl. Phys. **83**, 5447 (1998).
[21]T. Pisarkiewicz and A. Kolodziej, Phys. Status Solidi B **158**, K5 (1990).
[22]R. J. Mendelsberg, "Photoluminescence of ZnO grown by eclipse pulsed laser deposition," Ph.D. thesis (University of Canterbufy, New Zealand, 2009).
[23]F. Ruske, A. Pflug, V. Sittinger, B. Szyszka, D. Greiner, and B. Rech, Thin Solid Films **518**, 1289 (2009).
[24]E. Burstein, Phys. Rev. **93**, 632 (1954).
[25]T. S. Moss, Proc. Phys. Soc. B **67**, 775 (1954).
[26]G. Beni and T. Rice, Phys. Rev. B **18**, 768 (1978).
[27]D. C. Reynolds, D. C. Look, and B. Jogai, Solid State Commun. **99**, 873 (1996).
[28]J. Lu, S. Fujita, T. Kawaharamura, H. Nishinaka, Y. Kamada, T. Ohshima, Z. Ye, Y. Zeng, Y. Zhang, L. Zhu *et al.*, J. Appl. Phys. **101**, 083705 (2007).
[29]S. Jain, J. McGregor, and D. Roulston, J. Appl. Phys. **68**, 3747 (1990).
[30]S. C. Jain and D. J. Roulston, Solid State. Electron. **34**, 453 (1991).
[31]J. Y. W. Seto, J. Appl. Phys. **46**, 5247 (1975).
[32]J. Bruneaux, H. Cachet, M. Fromnet, and A. Messad, Thin Solid Films **197**, 129 (1991).
[33]P. F. Carcia, R. S. McLean, M. H. Reilly, and G. Nunes, Appl. Phys. Lett. **82**, 1117 (2003).
[34]M. Kon, P. Song, Y. Shigesato, P. Frach, S. Ohno, and K. Suzuki, Jpn. J. Appl. Phys., Part 1 **42**, 263 (2003).
[35]T. A. Gessert, J. N. Duenow, T. Barnes, and T. J. Coutts, U.S. patent application 12/441,707 (2008).
[36]B. Johs, J. A. Woollam, C. M. Herzinger, J. Hilfiker, R. Synowicki, and C. L. Bungay, Crit. Rev. Opt. Sci. **CR72**, 29 (1999).
[37]R. J. Mendelsberg, Y. Zhu, and A. Anders, J. Phys. D: Appl. Phys. **45**, 425302 (2012).